A new low-cost and non-intrusive feet tracker

Sébastien Piérard[1], Rémy Phan-Ba[2], Shibeshih Belachew[2], Marc Van Droogenbroeck[1]

✉[1]INTELSIG Laboratory, Montefiore Institute, University of Liège, Belgium
✉[2] MYDREAM, Department of Neurology, University Hospital of Liège, Belgium
Sebastien.Pierard@ulg.ac.be, Remy.PhanBa@chu.ulg.ac.be, SBelachew@ulg.ac.be, M.VanDroogenbroeck@ulg.ac.be

***Abstract*—Capturing gait is useful for many applications, including video-surveillance and medical purposes. The most common sensors used to capture gait suffer from significant drawbacks. We have therefore designed a new low-cost and non-intrusive system to capture gait. Our system is able to track the feet on the horizontal plane in both the stance and the swing phases by combining measures of several range laser scanners. The number of sensors can be adjusted according to the target application specifications. The first issue addressed in this work is the calibration: we have to know the precise location of the sensors in a plane, and their orientations. The second issue addressed is how to calculate feet coordinates from the distance profiles given by the sensors. Our method has proven to be robust and precise to measure gait abnormalities in various medical conditions, especially neurological diseases (with a focus on multiple sclerosis).**

***Index Terms*—gait analysis, gait recognition, multiple sclerosis, range laser scanners**

I. INTRODUCTION

Capturing gait is useful for many applications, such as person [1], gender [2], or age [3] identification. Gait analysis is also useful for medical purposes, since ambulation impairment is a frequent symptom of a broad range of diseases, including multiple sclerosis where quantitative evaluation of gait performances is a good indicator of disease activity.

The most common sensors used to capture gait are cameras (*cf* [4], [5], [6]), electronic walkways (such as the GAITRite [7]), and motion capture systems (*e.g.* Coda Motion units CX1 [8]). All these systems present significative drawbacks such as unreliability of the information obtained with color cameras since it depends on lighting conditions. The GAITRite system is expensive and provides only information regarding the position of the feet in the stance phase. Motion capture (mocap) systems are also expensive and require that the users wear (active or passive) tags, which is not possible in most applications.

We have designed a new system to capture gait. As feet paths are highly informative for gait recognition [9] and most of medical gait-based purposes, our aim is to determine the position of the feet in real time. Each foot is considered as a point in an horizontal plane, and the vertical movements are ignored. Many useful informations may be easily extracted: walking speed, distance between feet over time, swing phase duration, gait asymmetry, etc.

We use several range laser scanners to analyze an horizontal slice of the scene. Our platform is cheaper than existing motion capture systems and GAITRites, is insensitive to lighting conditions, and does not require the persons to wear any tag. Moreover, it captures the feet positions in both the swing and the stance phases.

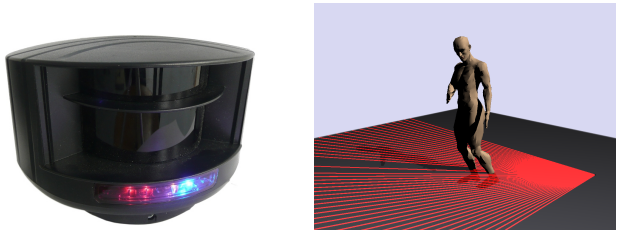

Figure 1. Our feet tracker is based on the distance profiles provided by a set of range laser scanners (*e.g. BEA LZR-i100*) placed in a horizontal plane.

The outline of this paper is as follows. Section II describes the selected sensors, their advantages, and their limitations. In Section III, we detail how our system is calibrated: the precise location of the sensors in a plane and their orientations are to be determined. Section IV is devoted to the tracker itself: it describes the way feet (*i.e.* ankle section plane) coordinates are calculated from the depth profiles given by the sensors. Section V focuses on the use of our tracker in a real medical application. Finally, we give a short conclusion in Section VI.

II. SENSORS

We use several range laser scanners to analyze an horizontal slice of the scene. The number of sensors can be adjusted according to the target application specifications. Using several sensors allows us to reduce occlusions, or to cover a wider area. The scanned plane is chosen to be located at $15\,cm$ above the floor, which is right above the tibio-tarsal joint of the ankle in a barefoot configuration for adult individuals in stance phase, and remains above the maximal height reached by the feet during the swing phase, allowing the range laser scanners to track the feet even in the swing phase.

A. Selecting the sensors

In previous works [10], [11], we used the range laser scanners *BEA LZR-p200*. Those sensors have been designed to monitor a door of $4\,m$ wide and $4\,m$ high, and therefore their behavior is undefined when the distances to measure exceed $4\sqrt{2} = 5.65\,m$. For some applications, it is mandatory to reach larger distances. For example, the $25\,ft$ distance ($7.62\,m$) is a common requirement for standardized tests concerning multiple sclerosis. That is why, in this work, we

have chosen another model of the same family: the *BEA LZR-i100* (see Figure 1). These have only a limit distance of $10\sqrt{2} \simeq 14.14\,m$, which is large enough for most applications.

The selected sensors are adequate for measuring distances with a high precision, without any reflector. They are small, and easy to place in various environments. Note that the risk of interference between sensors is negligible, and therefore it is safe to use several sensors to scan the same plane.

The sensors measure distances in 274 directions spanning $96°$, in a plane, at $15\,Hz$. Their resolution is $1\,mm$. In practice, we observe a temporal variation of a few millimeters, and seldom a few centimeters, on the acquired distances. It should be noted that the sensors are strongly disturbed by highly reflective materials such as metal, and black materials (in the infrared band). It should also be noted that at discontinuities, the sensors provide a random measure between the minimum and the maximum distance. Therefore, the sensors may see points where there is no object in the scene (these points are named *outliers* in the following). Robustness to outliers is therefore mandatory.

B. Behavior in dynamical scenes

The field of view of $96°$ is obtained thanks to an internal rotating mirror. As the mirror has to turn $48°$ to cover the $96°$, a frame is acquired in $\frac{1}{15}\cdot\frac{48}{360}\,s \simeq 9\,ms$.

An object of $10\,cm$ (*i.e.* the typical size of a leg) located at $1\,m$ from the sensor is viewed inside of a $5.7°$ large angle, and therefore in $\frac{5.7}{2}\frac{1}{15}\frac{1}{360}\,s \simeq 0.52778\,ms$. For a walking speed of $5\,km/h$, the maximal speed of the feet is approximately $16\,km/h$. In consequence, a foot can move by $\frac{0.52778}{1000}\frac{1600000}{3600} \simeq 0.235\,cm$ during the data acquisition. As this displacement is negligible, the selected sensors are quick enough to track feet with high precision.

However, it should be stressed that there exist no ways to synchronize the sensors. With multiple sensors, merging the information provided by the sensors is required. Unfortunately, there may be a temporal gap of $\frac{1}{15}\,s$ between the data to be fused. For a walking speed of $5\,km/h$, this is equivalent to an uncertainty of $29.6\,cm$ on a foot position in the worst case. Clearly, this source of uncertainty is dominant. Note however that this uncertainty is only along the path followed by the foot.

C. Towards a simple model of the sensors

In this paper, we assume that the sensors are punctual. This implies that the 274 lines-of-sight are concurrent and that the intersection point is located in the sensor. Under these assumptions, the distance measured between the sensor and a visible point of the scene is the distance between the point and the aforementioned intersection. It follows that, to obtain the coordinates of the 274 points seen by a sensor, a simple polar to cartesian transform suffices.

III. THE CALIBRATION PROCEDURE

The goal of the calibration procedure is to determine the precise location of the sensors in the room, and their orientations. This knowledge is mandatory to fuse the information provided by different sensors. Of course, this procedure has to be done only once, after the installation of the sensors in the room. In this section, we present a semi-automatic calibration procedure.

It should be stressed that the calibration has to be very accurate. An error of $0.075°$ on the orientation of a sensor has for consequence an error of $1\,cm$ on the location of a point seen at $7.62\,m$. A well designed calibration procedure is therefore needed.

A. Description of our calibration procedure

In the proposed procedure, a cylinder is successively placed in the room at a few places. Each sensor has its own local cartesian coordinate system. Each time the cylinder is displaced, its center coordinates are estimated in the local coordinate system of each sensor.

The passage from one local coordinate system to another is done by a transformation composed of translation and rotation. The calibration is equivalent to determining these transformations. The cylinder has to be placed a least at two different locations, but repeating the operation a dozen of times, to take advantage of the least squares error reduction mechanism, helps to improve the calibration. Note that there is no need to increase the number of locations if the number of sensors increases. Also, we assume that the cylinder is visible to all sensors.

Let $\left(C^s_{xi}, C^s_{yi}\right)$ be the coordinates of the cylinder in its i-th position expressed in the local cartesian coordinate system of sensor s. If, in the local cartesian coordinate system of sensor 0, the sensor s is located at $\left(\Delta^s_x, \Delta^s_y\right)$ and is looking in the direction θ^s, we have $\forall i$

$$\begin{pmatrix} \cos(\theta^s) & -\sin(\theta^s) & \Delta^s_x \\ \sin(\theta^s) & \cos(\theta^s) & \Delta^s_y \end{pmatrix} \begin{pmatrix} C^s_{xi} \\ C^s_{yi} \\ 1 \end{pmatrix} = \begin{pmatrix} C^0_{xi} \\ C^0_{yi} \end{pmatrix} \quad (1)$$

Therefore, the position and the orientation of the sensor s can be found solving the following linear equation:

$$\begin{pmatrix} C^s_{x0} & -C^s_{y0} & 1 & 0 \\ \vdots & \vdots & \vdots & \vdots \\ C^s_{xp} & -C^s_{yp} & 1 & 0 \\ C^s_{y0} & C^s_{x0} & 0 & 1 \\ \vdots & \vdots & \vdots & \vdots \\ C^s_{yp} & C^s_{xp} & 0 & 1 \end{pmatrix} \underbrace{\begin{pmatrix} \cos(\theta^s) \\ \sin(\theta^s) \\ \Delta^s_x \\ \Delta^s_y \end{pmatrix}}_{\text{unknowns}} = \begin{pmatrix} C^0_{x0} \\ \vdots \\ C^0_{xp} \\ C^0_{y0} \\ \vdots \\ C^0_{yp} \end{pmatrix} \quad (2)$$

As this system is overconstrained when the cylinder is placed more than two times, the solution has to be determined in the least-squares sense.

In practice, we manage to ensure that the cylinder is the only moving object in the scene during calibration. We apply a background subtraction to the signal provided by each sensor, in order to filter out the static elements of the scene and to keep only the points corresponding to the cylinder. To decrease the sensitivity to outliers, our implementation uses the RANSAC algorithm to obtain robust circle fits.

The remainder of this section is devoted to the comparison of four circle fitting procedures (three well known and a new one), and to the selection of the best one. In our case, the data points are sampled along a small arc of circle.

B. Circle fitting methods

Let (x_1, y_1), (x_2, y_2), $\dots$ (x_n, y_n) be the points by which we want to get a circle of radius R and center (C_x, C_y) to pass trough. The key to a solution consists in finding an optimization criterion that leads to equations easy to solve. For example, the least squares criterion

$$\min \sum_{i=1}^{n} \left(\sqrt{(x_i - C_x)^2 + (y_i - C_y)^2} - R \right)^2 \qquad (3)$$

is difficult to handle since it leads to a nonlinear problem that has no closed form solution (with iterative methods, one is faced with questions related to convergence, plateaus, valleys, and to the initial guess). Surprisingly, fitting a circle to a cloud of points is a difficult problem. A entire book devoted to the subject has been published recently [12].

1) KÅSA*'s method:* Instead of the criterion (3), KÅSA proposed in [13] to use the criterion

$$\min \sum_{i=1}^{n} \left((x_i - C_x)^2 + (y_i - C_y)^2 - R^2 \right)^2 \qquad (4)$$

Both criterions (3) and (4) are equivalent if there exists a circle passing through all points. However, the solution may be different if the observations are noisy. If R is an unknown, KÅSA's criterion is easier to deal with, because it leads to a unique and explicit solution. We denote the centered moments:

$$\mu_{ab} = \frac{1}{n} \sum_{i=1}^{n} (x_i - \bar{x})^a (y_i - \bar{y})^b \qquad (5)$$

where $\bar{x} = \frac{1}{n}\sum_{i=1}^{n} x_i$ and $\bar{y} = \frac{1}{n}\sum_{i=1}^{n} y_i$ are the coordinates of the gravity center of the cloud of points. With KÅSA's criterion, the optimal center of the circle is given by

$$C_x = \bar{x} + \frac{1}{2} \frac{\mu_{02}(\mu_{30} + \mu_{12}) - \mu_{11}(\mu_{03} + \mu_{21})}{\mu_{20}\mu_{02} - \mu_{11}^2} \qquad (6)$$

$$C_y = \bar{y} + \frac{1}{2} \frac{\mu_{20}(\mu_{03} + \mu_{21}) - \mu_{11}(\mu_{30} + \mu_{12})}{\mu_{20}\mu_{02} - \mu_{11}^2} \qquad (7)$$

2) Our method: KÅSA*'s criterion with* R *known:* If the radius is known, then the optimal center corresponding to KÅSA's criterion may differ because we cannot write anymore

$$\frac{\partial}{\partial R} \sum_{i=1}^{n} \left((x_i - C_x)^2 + (y_i - C_y)^2 - R^2 \right)^2 = 0 \qquad (8)$$

Without loss of generality, let's assume that $\bar{x} = 0$ and $\bar{y} = 0$. This can be obtain by translation the cloud of points if needed. The center can be found by solving the following system.

$$\begin{cases} \frac{\partial}{\partial C_x} \sum_{i=1}^{n} \left((x_i - C_x)^2 + (y_i - C_y)^2 - R^2 \right)^2 &= 0 \\ \frac{\partial}{\partial C_y} \sum_{i=1}^{n} \left((x_i - C_x)^2 + (y_i - C_y)^2 - R^2 \right)^2 &= 0 \end{cases} \qquad (9)$$

$$\Leftrightarrow \begin{cases} C_x \left(3\mu_{20} + \mu_{02} - R^2\right) + C_x^3 + C_x C_y^2 + C_y \left(2\mu_{11}\right) \\ \qquad = \mu_{30} + \mu_{12} \\ C_x \left(2\mu_{11}\right) + C_y^3 + C_x^2 C_y + C_y \left(3\mu_{02} + \mu_{20} - R^2\right) \\ \qquad = \mu_{03} + \mu_{21} \end{cases}$$

At first sight, solving this system is difficult because the equations are of the third order. Let's assume that the distance between the gravity center of the cloud and the center of the circle is known, that is $C_x^2 + C_y^2 = \Delta$, and using Cramer's rule,

$$\Leftrightarrow \begin{cases} C_x &= \frac{(\mu_{30}+\mu_{12})\left(3\mu_{02}+\mu_{20}-R^2+\Delta\right)-(\mu_{03}+\mu_{21})(2\mu_{11})}{(3\mu_{20}+\mu_{02}-R^2+\Delta)(3\mu_{02}+\mu_{20}-R^2+\Delta)-4\mu_{11}^2} \\ C_y &= \frac{(\mu_{03}+\mu_{21})\left(3\mu_{20}+\mu_{02}-R^2+\Delta\right)-(\mu_{30}+\mu_{12})(2\mu_{11})}{(3\mu_{20}+\mu_{02}-R^2+\Delta)(3\mu_{02}+\mu_{20}-R^2+\Delta)-4\mu_{11}^2} \end{cases}$$

Of course, the value of Δ has to be determined. This can be done by checking that $C_x^2 + C_y^2 = \Delta$ as assumed. With a few simple algebraic manipulations, one can check that Δ is a root of a fifth order polynomial

$$\Delta^5 + k_4\Delta^4 + k_3\Delta^3 + k_2\Delta^2 + k_1\Delta + k_0 = 0 \qquad (10)$$

The values of k_0, k_1, k_2, k_3, and k_4 are not given here due to a lack of space, but can be easily computed. There are at most 5 solutions, and selecting the best one can be done using KÅSA's criterion. Only the positive roots should be considered, as Δ is positive by definition. Note also that there exists always at least one solution, even if the sample points are collinear, because $k_0 \leq 0$[1].

3) The methods of PRATT *and* TAUBIN*:* Instead of parametrizing a circle with $\{C_x, C_y, R\}$, PRATT [14] proposed to use $\{A, B, C, D\}$ such that the equation of the circle is

$$A\left(x^2 + y^2\right) + Bx + Cy + D = 0 \qquad (11)$$

This parameterization allows to describe circles as well as lines (with $A = 0$). In some cases, only a small arc of the circle is observed and it is hazardous to estimate the radius and to decide on which side of the cloud the circle is. In those cases, some people (*e.g.* [12]) prefer to fit a line instead of a circle. The criterion related to this parameterization is

$$\min \sum_{i=1}^{n} \left(A\left(x_i^2 + y_i^2\right) + Bx_i + Cy_i + D \right)^2 \qquad (12)$$

Because the parameters $\{A, B, C, D\}$ are defined up a scale factor, and to avoid the trivial solution $A = B = C = D = 0$, one has to add a constraint. It can be showed that KÅSA's criterion is equivalent to this one with the constraint $A = 1$. PRATT [14] used the constraint $B^2 + C^2 - 4AD = 1$ which has the advantage of ensuring that $B^2 + C^2 - 4AD > 0$ (this is required for circles). TAUBIN [15] proposed

$$\frac{4A}{n} \sum_{i=1}^{n} \left(A\left(x_i^2 + y_i^2\right) + Bx_i + Cy_i + D \right) + \left(B^2 + C^2 - 4AD\right) = 1 \qquad (13)$$

Other constraints have also be proposed by Gander [16] and Nievergelt [17], but we will not consider them in this paper.

C. Selection of the circle fitting method

We evaluated the four above-mentionned methods (KÅSA, KÅSA with R known, TAUBIN, and PRATT) by simulation. For the methods of PRATT and TAUBIN, we have used the publicly available implementation of the author of [12][2].

[1] The polynomial takes a negative value for $\beta = 0$, and a positive infinite one for $\beta = +\infty$. Therefore, there is at least one root between 0 and $+\infty$.

[2] http://www.math.uab.edu/~chernov/cl/MATLABcircle.html

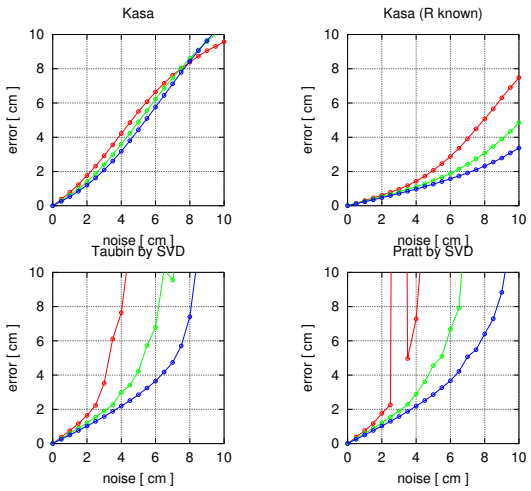

Figure 2. The mean distance between the estimated center of the calibration cylinder and its true center, as a function of the noise level u. The red, green, and blue curves correspond respectively to a calibration cylinder with a diameter of 30 cm, 40 cm, and 50 cm. These results show that the fit method introduced in this paper (solving KÅSA's criterion with R known) outperforms the other ones (the methods of KÅSA, TAUBIN and PRATT).

A cylinder is placed randomly, and fully included in the visual field of the sensor. It is separated from the sensor by a distance between 50 cm and 10 m. A noise was simulated on the distances measured by the virtual sensor: each measurement is corrupted independently of the others, and the noise is distributed uniformly on the$[-u, u]$ interval. Therefore, we assume that the distance measures are unbiased. We observe the mean error, *i.e.* the mean distance between the estimated center of the calibration cylinder and its true center. We want to select the fitting method with the lower mean error. The mean error depending on the noise level is depicted in Figure 2.

Note that KÅSA's method is known to be highly biased when a small arc is sampled. This bias is difficult to compensate, because it depends on the noise level, and the sensors are insufficiently characterized to predict the noise level.

Our experiments have shown that KÅSA with R known is the fitting method that is best suited to our particular case. KÅSA with R known is less sensitive to noise than KÅSA. The methods of PRATT and TAUBIN are almost equivalent, and are unable to cope with important noise (whether one uses a SVD or Newton's method). The reason is probably that fitting lines as well as circles in a bad idea in our case because $C_x = -\frac{B}{2A}$ and $C_y = -\frac{C}{2A}$. Therefore, if the fitting method prefers a line, estimating C_x and C_y is impossible since $A = 0$. This conclusion stands in deep contrast with the one of [12], which stated that the methods PRATT and TAUBIN are theoretically preferable to KÅSA's one, as a general rule.

D. Remark: application to robotics

Fitting circles of known radius to points sampled along a small arc is a problem often encountered in robotics. For example, in [18], a mobile robot should interact with known objects that have a cylindrical base. The sensor is a range laser scanner or a 3D camera, and therefore the localization of the objects is equivalent to the estimation of the object center from a set of points sampled along an arc of circle. This is exactly the same problem we are facing here. In [18] the circle is fitted with KÅSA's method; we know now that it is not the best choice and that using KÅSA's criterion with R known would be a lot more precise.

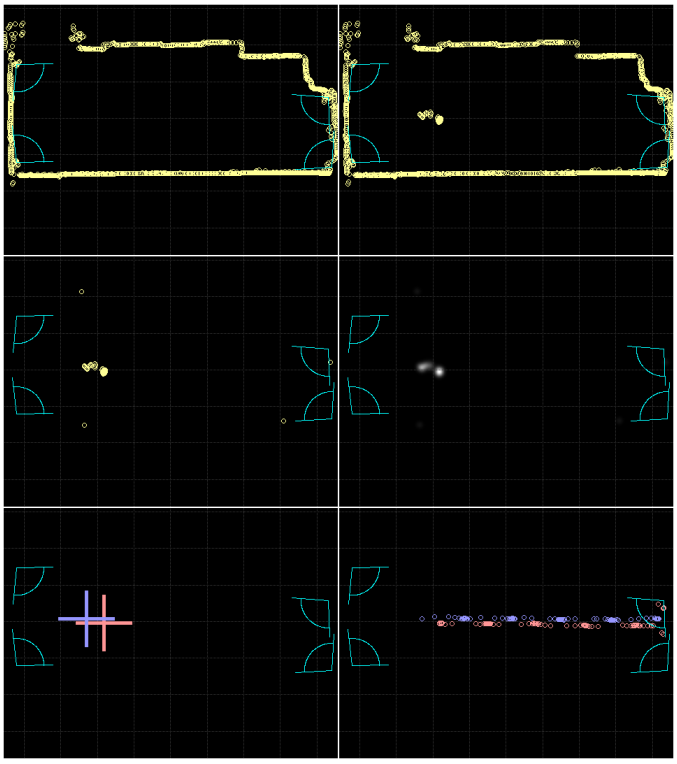

Figure 3. The different steps of our method. From the top left picture to the bottom right one: (1) the model of the empty scene, *i.e.* the background (2) the points seen by all sensors (3) the result of the background subtraction (4) after the convolution with a gaussian kernel (5) after local maxima search (6) the final result of the tracker.

IV. THE FEET TRACKER

The most straightforward methodology to track the feet consists in building a localization map (*cf* [10]), filtering uninteresting static objects (chairs, tables, ...) by using a background subtraction algorithm (such as [19]), and isolating the feet by a connected components analysis (such as [20]). However, the technique proposed in [10] to combine the information provided by several range laser scanners assumes that the observed scene is nearly static, and that the sensors don't see outlier points. Unfortunately, this is not the case, so we propose a new method. Its main steps are depicted in Figure 3.

A. Locating the feet

Each sensor sees a cloud of points in the horizontal plane. Thanks to the calibration, these clouds can be superimposed, and merged. From the resulting cloud, we have to estimate a set of two points that are the centers of each foot (or leg).

We apply a background subtraction to the signal provided by each sensor, in order to filter out the static elements of the scene and to keep only the points corresponding to the

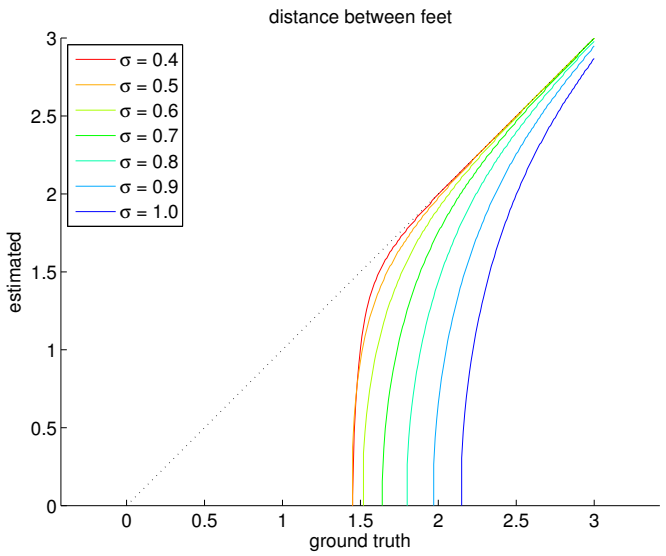

Figure 4. The theoretical error on the feet positions. The unit chosen to express the distances and σ is such that the diameter of the leg is $D = 1$. These curves have been obtained by simulation in noise-free conditions, with uniform and dense sampling.

feet. Then, the remaining points are convolved with a gaussian kernel of standard deviation σ (*i.e.* a gaussian is placed at each each point, and they are summed). We expect to have, in most cases, the two largest local maxima where the feet are. We do not provide any output if there is less than two local maxima, or if they are spaced more than it is possible. This method is robust to outliers, and therefore a simple background subtraction method suffices.

The standard deviation σ is the only parameter that has to be chosen. For the sake of theory, let's assume that the horizontal section of the feet are circles, and that they are uniformly sampled. Let's denote D the diameter of the feet.

We want to get a local maximum per foot. If there was only one foot in the scene, it can be showed that σ should be larger than $\frac{D}{2}$ if the sensors see only two points of the feet, or larger than $0.36\,D$ if the sensors see a lot of points. Now, consider two feet. If σ is too large, there is a risk to observe only one maximum for both feet. The fact that we observe one or two maxima depends on the distance between the feet, on D and on σ. This relation is depicted in Figure 4. We consider that, in the worst case, $D = 14\,cm$ (with trousers) and that only two points are seen by foot. Accordingly, we chose $\sigma = \frac{D}{2} = 7\,cm$. According to Figure 4, we expect our localization procedure to fail if the distance between the centers of the legs is less than $14 \times 1.4428 \simeq 20\,cm$ and to give a biased result if the distance is less than $14 \times 2 \simeq 28\,cm$.

In future work, we would like to improve the localization procedure in order to obtain an unbiased feet position estimate, and to be able to localize the feet even if there are close. Some ideas are (i) to correct the estimate thanks to the known relation between the estimated inter-feet distance and its true value, or (ii) to use a gaussian ring kernel instead of the gaussian one, or (iii) to use machine learning principles.

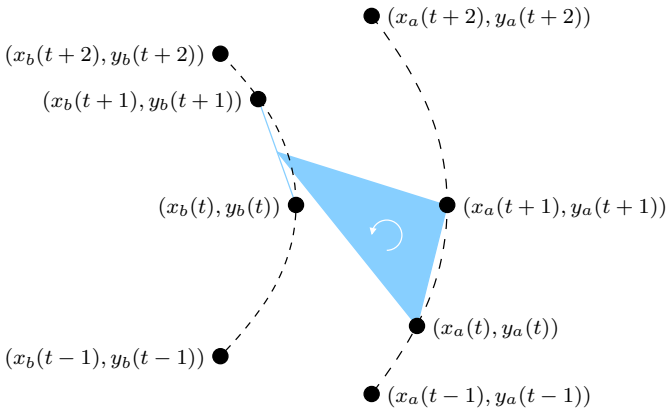

Figure 5. $\Phi_{ab}(t)$ is the signed area of the blue triangle.

B. *Tracking the feet*

At this point, we have a couple of points at each frame. In this step, we would like to cluster all the points in two classes, in order to obtain a trajectory for each foot.

At the time this paper is written, we minimize the total length of the two trajectories. This criterion leads to excellent results when the observed person walks along a line. However, from time to time we observed that when the person turns quickly, the trajectories may cross. This is probably due to an insufficient acquisition rate ($15\,Hz$). This kind of problem also arises with a tandem gait walk. In future work, we plan to improve the technique used to track the feet, perhaps using a Kalman filter.

C. *Identifying the feet*

We know the position of both feet over time, but we still need to determine which foot is the left one, and which one is the right one. The only clue available is the motion direction. Therefore, it is impossible to correctly identify the feet if the observed person moves in reverse. Let's denote $(x_f(t), y_f(t))$ the coordinates of the foot "f" at time t. The following quantity

$$\Phi_{ab}(t) = \frac{1}{2} \begin{vmatrix} x_a(t) & x_a(t+1) & \frac{x_b(t)+x_b(t+1)}{2} \\ y_a(t) & y_a(t+1) & \frac{y_b(t)+y_b(t+1)}{2} \\ 1 & 1 & 1 \end{vmatrix} \tag{14}$$

is positive if the foot "a" is on the right of the foot "b" between the times t and $t+1$, and $|\Phi_{ab}(t)|$ is a certainty factor (the geometrical meaning of $\Phi_{ab}(t)$ is depicted in Figure 5). Therefore, letting T be the total walk duration,

$$\sum_{t=0}^{T-2} \left[\Phi_{12}(t) - \Phi_{21}(t)\right] < 0 \tag{15}$$

if the trajectory number 1 corresponds to the left foot. We expect this criterion to be suitable, not only for straight paths, but also for any path (such as an $\circ$-shaped path or an ∞-shaped path).

V. APPLICATION TO NEUROLOGICAL DISEASE ANALYSIS

Gait disorders measurement and quantification is of the utmost importance in the follow-up and therapeutic decision-making process of numerous medical conditions (whether

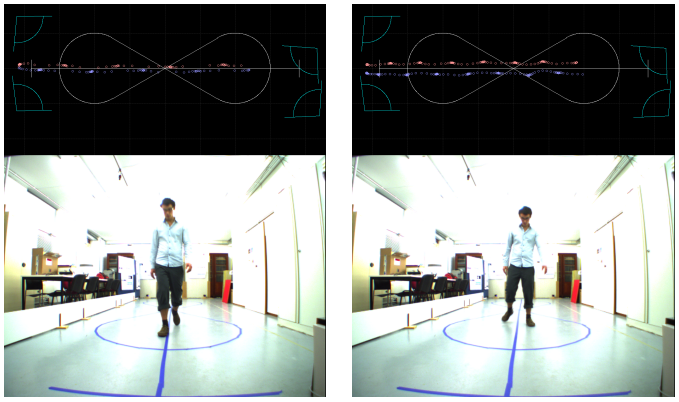

Figure 6. Screenshots of our software. Upper images display the position of the four sensors (obtained by calibration), a $25\,ft$ straight path, and the previously estimated feet positions. On the left hand side, the observed person has a normal gait, and on the right hand side, he has an ataxic gait. Such pathologies can be easily detected and measured with our method. A few full videos are available at http://www.ulg.ac.be/telecom/vgaims/.

orthopaedic, rhumatologic, pediatric, cardiorespiratory, or neurologic). For example, in the field of multiple sclerosis, a common neurological disease where gait is frequently impaired, change in walking performances can lead to significative therapeutic modifications [21].

However, the current available tools measuring gait dysfunction suffer from various limitations [22] and are completely blind to certain important gait features, such as ataxia, symmetry of the feet paths and individual feet walking speed, freezing of gait, etc, that are only qualitatively described in the neurological examination. The feet tracker developed in this work allows one to easily capture these features in a simple way, and at low cost (see Figure 6).

A dozen of videos demonstrating our results are available at http://www.ulg.ac.be/telecom/vgaims/. Qualitatively, our method is robust and precise. It is clear beyond the traditional measurement of global walking speed, and its use can be extended to measure more subtle and specific gait abnormalities. However, the questions of precision and accuracy are still problematic, because of the intrinsic lack of ground-truth data in this specific field.

VI. CONCLUSION

We have developed a new platform to capture gait, and a dedicated calibration procedure. It is a non-intrusive and low-cost platform. It has proven to be suitable for medical purposes, and we think that it can be used for other applications like automatic person identification.

REFERENCES

[1] N. Boulgouris, D. Hatzinakos, and K. Plataniotis, "Gait recognition: a challenging signal processing technology for biometric identification," *IEEE Signal Processing Magazine*, vol. 22, no. 6, pp. 78–90, November 2005.

[2] X. Li and S. Yan, "Gait components and their application to gender recognition," *IEEE Transactions on Systems, Man, and Cybernetics – Part C: Applications and Reviews*, vol. 38, no. 2, pp. 145–155, March 2008.

[3] J. Lu and Y.-P. Tan, "Gait-based human age estimation," *IEEE Transactions on Information Forensics and Security*, vol. 5, no. 4, pp. 761–770, December 2010.

[4] O. Barnich and M. Van Droogenbroeck, "Frontal-view gait recognition by intra- and inter-frame rectangle size distribution," *Pattern Recognition Letters*, vol. 30, no. 10, pp. 893–901, July 2009.

[5] B. McDonald and R. Green, "A silhouette based technique for locating and rendering foot movements over a plane," in *International Conference on Image and Vision Computing*, Wellington, New Zealand, November 2009, pp. 385–390.

[6] E. Stone, D. Anderson, M. Skubic, and J. Keller, "Extracting footfalls from voxel data," in *International Conference of the Engineering in Medicine and Biology Society (EMBC)*, Buenos Aires, Argentina, August-September 2010, pp. 1119–1122.

[7] U. Givon, G. Zeilig, and A. Achiron, "Gait analysis in multiple sclerosis: Characterization of temporal-spatial parameters using gaitrite functional ambulation system," *Gait & Posture*, vol. 29, no. 1, pp. 138–142, 2009.

[8] C. Schwartz, B. Forthomme, O. Brüls, V. Denoël, S. Cescotto, and J. Croisier, "Using 3D to understand human motion," in *Proceedings of 3D Stereo MEDIA*, Liège, Belgium, December 2010.

[9] A. Świtoński, A. Polański, and K. Wojciechowski, "Human identification based on gait paths," in *Advances Concepts for Intelligent Vision Systems (ACIVS)*, ser. Lecture Notes in Computer Science, J. Blanc-Talon, R. Kleihorst, W. Philips, D. Popescu, and P. Scheunders, Eds., vol. 6915. Gent, Belgium: Springer, August 2011, pp. 531–542.

[10] S. Piérard, V. Pierlot, O. Barnich, M. Van Droogenbroeck, and J. Verly, "A platform for the fast interpretation of movements and localization of users in 3D applications driven by a range camera," in *3DTV Conference*, Tampere, Finland, June 2010.

[11] O. Barnich, S. Piérard, and M. Van Droogenbroeck, "A virtual curtain for the detection of humans and access control," in *Advanced Concepts for Intelligent Vision Systems (ACIVS), Part II*, Sydney, Australia, December 2010, pp. 98–109.

[12] N. Chernov, *Circular and linear regression: fitting circles and lines by least squares*, ser. Chapman & Hall/CRC Monographs on Statistics & Applied Probability. USA: CRC Press, 2011, vol. 117.

[13] I. Kåsa, "A circle fitting procedure and its error analysis," *IEEE Transactions on instrumentation and measurement*, vol. IM-25, no. 1, pp. 8–14, March 1976.

[14] V. Pratt, "Direct least-squares fitting of algebraic surfaces," in *Proceedings of the 14th annual conference on Computer graphics and interactive techniques (SIGGRAPH)*, vol. 21(4), July 1987, pp. 145–152.

[15] G. Taubin, "Estimation of planar curves, surfaces, and nonplanar space curves defined by implicit equations with applications to edge and range image segmentation," *IEEE Transactions on Pattern Analysis and Machine Intelligence*, vol. 13, no. 11, pp. 1115–1138, November 1991.

[16] W. Gander, G. Golub, and R. Strebel, "Least-squares fitting of circles and ellipses," *BIT Numerical Mathematics*, vol. 34, no. 4, pp. 558–578, 1994.

[17] Y. Nievergelt, "Hyperspheres and hyperplanes fitted seamlessly by algebraic constrained total least-squares," *Linear Algebra and its Applications*, vol. 331, pp. 43–59, 2001.

[18] M. Greuter, M. Rosenfelder, M. Blaich, and O. Bittel, "Obstacle and game element detection with the 3d-sensor kinect," in *Research and Education in Robotics - EUROBOT 2011*. Springer, 2011, vol. 161, pp. 130–143.

[19] O. Barnich and M. Van Droogenbroeck, "ViBe: A universal background subtraction algorithm for video sequences," *IEEE Transactions on Image Processing*, vol. 20, no. 6, pp. 1709–1724, June 2011.

[20] F. Chang, C.-J. Chen, and C.-J. Lu, "A linear-time component-labeling algorithm using contour tracing technique," *Computer Vision and Image Understanding*, vol. 93, no. 2, pp. 206–220, February 2004.

[21] A. Goodman, T. Brown, L. Krupp, R. Schapiro, S. Schwid, R. Cohen, L. Marinucci, and A. Blight, "Sustained-release oral fampridine in multiple sclerosis: a randomised, double-blind, controlled trial," *The Lancet*, vol. 373, no. 9665, pp. 732–738, February 2009.

[22] R. Phan-Ba, A. Pace, P. Calay, P. Grodent, F. Douchamps, R. Hyde, C. Hotermans, V. Delvaux, I. Hansen, G. Moonen, and S. Belachew, "Comparison of the timed 25-foot and the 100-meter walk as performance measures in multiple sclerosis," *Neurorehabilitation and neural repair*, vol. 25, no. 7, pp. 672–679, September 2011.